Wide-Band Channel Sounding at 24 GHz Based on a Novel Fiber-Optic Synchronization Concept

Pascal Truffer, *Student Member, IEEE*, and Peter. E. Leuthold, *Member, IEEE*

***Abstract*—This paper describes a novel fiber-optic synchronization concept used in a versatile channel sounding system called the ETH channel sounder operating at 24 GHz (ECHO 24). ECHO 24 achieves a 2-ns path delay resolution and allows the measurement of complex channel impulse responses with Doppler frequencies $<$200 kHz based on a correlation method. Moreover, an antenna array together with an appropriate signal-processing scheme yields the angle of arrival of the impinging waves at the receiver (Rx) site. The intolerable frequency offset due to the operation of locally separated oscillators in the transmitter (Tx) and Rx can be overcome by a remote Tx and Rx supply with a common carrier generated in a control unit. The problem of line attenuation in coaxial cables at millimeter-wave frequencies is circumvented by the generation of appropriate optical signals, which are fed to the Tx and Rx via thin and flexible fibers. The absence of mixers and frequency multipliers yields rather small Tx and Rx modules and, therefore, reduces the deformation of the electromagnetic field to be investigated. ECHO 24 exhibits a dynamic range of 55 dB. Measurements are presented to demonstrate the versatility and precision of ECHO 24.**

***Index Terms*—Fiber-optic antenna feeding, time-variant radio channels, wide-band channel sounder.**

I. INTRODUCTION

EFFICIENT wireless indoor transmission represents a key technology to pave the way toward the realization of universal personal telecommunications (UPT) [1]. Various concepts and system platforms for broad-band wireless access in an indoor environment are under consideration in the European Advanced Communications Technologies and Services (ACTS) mobile programme [2], which include the following:

- wireless asynchronous transfer mode (ATM) for the transmission of information with data rates $>$20 Mbit/s at 5.2 and 17 GHz;
- high-speed wireless local area network (LAN) systems at 60 GHz; due to the absorption of oxygen, this frequency band is well suited for short range applications only with bit rates up to 155 Mb/s;
- mobile broad-band systems (MBSs) trial platform at 40 GHz offering bit rates of up to 34 Mb/s;
- wireless public access to broad-band-integrated services digital network (B-ISDN) services for low mobility terminals operating at 19 GHz.

Considering the potential of future wireless communication systems in the range of 10 to 60 GHz, the investigation of the radio channels in the industrial scientific medical (ISM) band at 24 GHz with a bandwidth up to 1 GHz seems to be an optimum choice.

The design of future wireless communication systems will be based on reliable channel models. They may serve for the prediction of the electromagnetic-field strength at a certain location, as well as for the performance evaluation of promising transmitter (Tx) and receiver (Rx) structures in order to maximize the capacity of the overall system. The development of reliable channel models gives rise to an increasing demand for precise radio-channel measurements, especially in complex picocellular environments. Due to the individual radiation pattern, the antennas of both the Tx and Rx have a major impact on the investigated radio channel. From a theoretical point-of-view, measurements should be performed by means of isotropic (omnidirectional) wide-band antennas. In practice, it is reasonable to use antennas with radiation patterns according to $\lambda/4$ monopoles, often applied in many wireless communication systems. In order to measure the complex channel impulse response (CIR), the coherence time of the radio channel has to exceed the measurement period. Other system functions, e.g., the delay Doppler-spread function, the time-variant transfer function, and the output Doppler-spread function can be calculated from the complex CIR since they are related by the Fourier transform [3]. The radio channel is characterized completely by one of these four system functions. Since adaptive antennas become more and more attractive to increase the capacity of broad-band wireless networks, array measurements are necessary to obtain directional information about the impinging waves due to multipath propagation. In this a case, each antenna element yields a CIR or a related system function, respectively. Deriving a model for a specific application, the parameters can be estimated from the ensemble of the CIRs. For this purpose, powerful signal-processing methods may often be required [4], [5].

Narrow- and wide-band measurements in indoor environments can be carried out by means of commercially available network analyzers if the radio channel is more or less time invariant during the measurement period [6], [7]. The investigation of time-variant radio channels, however, necessitates more elaborate measurement methods [8]. The channel sounder described in [9] makes use of a fast frequency sweep (chirp) for real-time measurements at 60 GHz with 5-ns delay resolution, whereby the sweep time is smaller than the coherence time of the channel. The UHF channel sounder developed at our laboratory about five years ago [10] is of a sliding correlator type and employs carriers modulated with pseudonoise (PN) sequences to perform measurements at 0.9 and 2 GHz with

Manuscript received January 21, 2000.

The authors are with the Communication Technology Laboratory, Swiss Federal Institute of Technology, CH-8092 Zurich, Switzerland (e-mail: truffer@nari.ee.ethz.ch).

Publisher Item Identifier S 0018-9480(01)02430-9.

10-ns delay resolution. The ETH channel sounder operating at 24 GHz (ECHO 24) represents the follow-up system with enhanced carrier frequency and increased bandwidth. Contrary to the online signal processing in the UHF channel sounder, the received signal is digitized, stored in a fast acquisition memory, and correlated offline.

Coherent demodulation is required to measure the complex CIR of the channel. For this purpose, the Tx and Rx of the UHF channel sounder has been equipped with a Rubidium atomic standard each. According to the manufacturer's specifications a time deviation error of 1.44 ps results for an Alan Variance of $\Delta f/f = \pm 2.5 \cdot 10^{-12}$ after 1 s. This value corresponds to an output frequency of 10 MHz and will be increased to 3.5 ns at 24 GHz, what leads to an intolerable phase jitter.

A remote feeding of the Tx antenna with the locally generated carrier signal solves this problem. Unfortunately, line attenuation at 24 GHz is significant; values of about 4 dB/m are typical for a modern semirigid coaxial cable. At 60 GHz, it would become even 7 dBm. In addition, the handling of stiff coaxial cables is rather cumbersome. Hence, a fiber-optic feeding concept has been chosen, which permits the realization of flexible and low attenuation links to the Tx antenna and the Rx and also circumvents the use of voluminous and costly mixer and frequency multiplier devices. Moreover, the compact hardware modules have only little influence on the wave propagation and, therefore, a higher precision of the complex CIR measurement can be achieved.

In Section II, the system concept with the fiber-optic synchronization link between Tx and Rx will be discussed in detail. Section III contains implementation aspects of the system, while in Section IV, the system performance is investigated. Different radio channel measurements performed with ECHO 24 are presented in Section V.

II. SYSTEM CONCEPT

In this section, the novel synchronization concept based on optical millimeter-wave generation [11] will be explained. The block diagram of the sounder system, which consists of a Tx and a Rx module both connected with an optical fiber to a control unit, is depicted in Fig. 1.

The Tx antenna is fed by the modulated millimeter-wave signal $u_c(t) = \Re\{u(t)e^{j2\pi f_c t}\}$ generated at the output of the photodetector (PD) at a carrier frequency $f_c = 24$ GHz, where $\Re\{\cdot\}$ denotes the real part and $u(t)$ is a periodically repeated bipolar PN code sequence with a chip rate of 500 MHz. The signals $y_{mc}(t)$ at the outputs of M antenna elements located in an array of a certain geometrical configuration are induced by the impinging partial waves at the Rx site. After a coherent demodulation with the unmodulated carrier also generated at the output of the PD in Rx, data of the complex amplitude, delay, and incident angle with regard to each transmission path result from signal postprocessing by suitable algorithms.

PDs designed for modulation frequencies ≤ 60 GHz are commercially available today, but analog lightwave modulators adapted to modulating signals in the range of 24 GHz up to 60 GHz are not yet on the market. A modern Mach–Zehnder interferometer (MZI) can be operated by signals up to 18 GHz. Hence, taking advantage of the nonlinear characteristic of the MZI [12], it is possible to generate modulated millimeter waves at 24 GHz while the frequency of the modulating signal stays well below 18 GHz. This method is subsequently described.

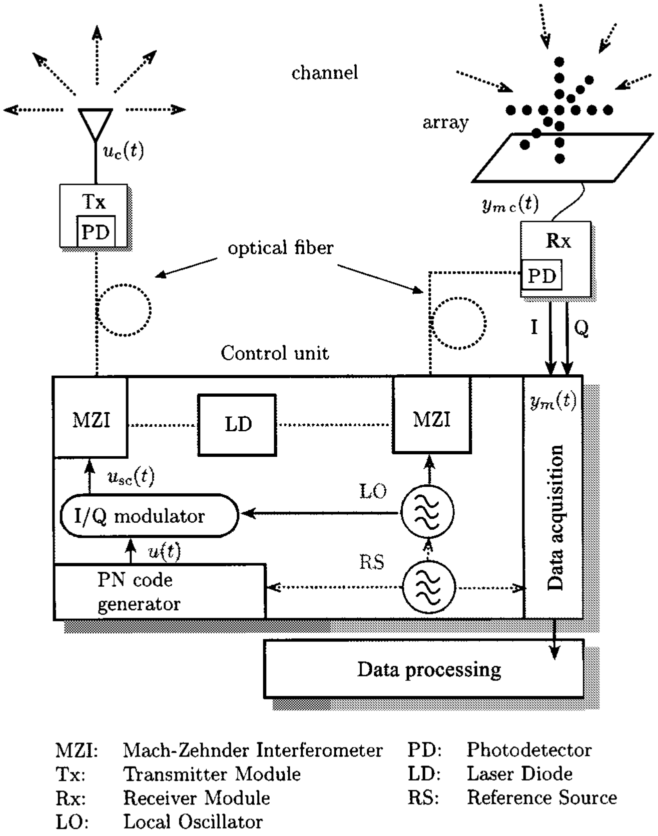

Fig. 1. Block diagram of the sounder system.

The optical output power of the MZI, i.e., the time-variant light intensity, is denoted by

$$P_{\mathrm{opt}}(t) = \frac{P_{\mathrm{laser}}}{2}\left[1+\cos\frac{\pi}{V_\pi}\left(V_{\mathrm{bias}}+u_{\mathrm{sc}}(t)\right)\right] \qquad (1)$$

where the symbols are as follows:

P_{laser}	average optical output power of the laser diode (LD);
V_{bias}	applied bias voltage;
V_π	extinction bias voltage;
$u_{\mathrm{sc}}(t)$	instantaneous input voltage.

The MZI is operated at the bias point $V_{\mathrm{bias}} = V_\pi$, where the phase difference of the signals in the two branches of the MZI equals π and, therefore, the optical carrier is completely suppressed. With $u_{\mathrm{sc}}(t) = A\cos(\phi(t))$, where A is the amplitude, (1) becomes

$$P_{\mathrm{opt}}(t) = \frac{P_{\mathrm{laser}}}{2}\left[1-\cos\left(\frac{\pi A}{V_\pi}\cos\left(\phi(t)\right)\right)\right]. \qquad (2)$$

Provided that $u_{\mathrm{sc}}(t)$ is a harmonic signal, i.e.,

$$\phi(t) = 2\pi f t + \varphi_0 \qquad (3)$$

(2) can be expanded into a Fourier series in order to determine the frequency content of $P_{\rm opt}(t)$ as follows:

$$P_{\rm opt}(t) = \frac{P_{\rm laser}}{2}\left(1 - J_0\left(\frac{\pi A}{V_\pi}\right) + 2J_2\left(\frac{\pi A}{V_\pi}\right)\cos\left(2\phi(t)\right)\right. \\ \left. -2J_4\left(\frac{\pi A}{V_\pi}\right)\cos\left(4\phi(t)\right) + \cdots\right. \quad (4)$$

The coefficients $J_{2n}(\pi A/V_\pi)$, $n = 0, 1, 2, \ldots$, represent the Bessel functions of order $2n$ with the argument $\pi A/V_\pi$. Obviously, only even harmonics occur. According to the physical property of a PD, the second harmonic generates an electrical output signal proportional to the time-variant light intensity or the quadratic light signal amplitude, respectively. The influence of higher order harmonics after conversion into the electrical domain can be neglected. From a theoretical point-of-view, the amplitude A of $u_{\rm sc}(t)$ should be chosen such that it maximizes the term $J_2(\pi A/V_\pi)$ in order to achieve maximum power. The applied MZIs can be operated with voltages in the range of -5 to $+5$ V.

The second harmonic gives rise to a doubling of the phase $\phi(t)$. Therefore, in order to obtain the signal $u_{\rm c}(t)$ with the phase $\phi_c(t) = 2\pi f_c t + u(t)(\pi/2)$, a special subcarrier modulation is needed to prepare a signal $u_{\rm sc}(t)$ with the phase $\phi(t) = 2\pi(f_c/2)t + u(t)(\pi/4)$. Such a 90° phase modulation can be performed by an in-phase/quadrature (I/Q) modulator (Fig. 1). The local oscillator (LO) signal at $f_c/2$ is modulated by the PN code applied to the Q input, while the I input is kept on a constant voltage equal to the amplitude of the PN code. For a rectangular PN code sequence $u(t)$ with amplitude ± 1, the subcarrier signal is as follows:

$$\begin{aligned} u_{\rm sc}(t) &= A\cos\left(2\pi\frac{f_c}{2}t + u(t)\frac{\pi}{4}\right) \\ &= \frac{A}{\sqrt{2}}\left[u(t)\sin\left(2\pi\frac{f_c}{2}t\right) + \cos\left(2\pi\frac{f_c}{2}t\right)\right]. \end{aligned} \quad (5)$$

For the sake of completeness, it should be mentioned that, according to (3), the modulation phase φ_0 means a constant, while $u(t)\pi/4$ represents a function of time. However, since the technical bandwidth of $u(t)$ (500 MHz) is small compared to the subcarrier frequency $f_c/2 = 12$ GHz, the Fourier expansion (4) may be considered as an acceptable approximation. The input/output relation of the PD is given by

$$i_{\rm pd}(t) = R \cdot P_{\rm opt}(t) \quad (6)$$

where $i_{\rm pd}(t)$ denotes the output current of the electrical signal and R is the responsivity of the PD. Expressing $P_{\rm opt}(t)$ by (4), the detected signal or the desired sounder signal $u_{\rm c}(t)$, respectively, results after a bandpass amplification directly as

$$u_{\rm c}(t) \sim i_{\rm pd}(t) \sim \cos\left(2\phi(t)\right) = \cos\left(2\pi f_c t + u(t)\frac{\pi}{2}\right). \quad (7)$$

The accuracy of channel measurements depends considerably on the quality of the carrier signal. A crucial property represents the carrier phase noise, which turns out to be low for the previously described optical signal generation method. In order to analyze the spectrum of the light that is fed to the Tx module, we derive the light field strength, e.g., the electric-field component from (2) by means of the following assumption:

$$\begin{aligned} E_{\rm opt}(t) &\sim \sqrt{P_{\rm opt}(t)}\cos(2\pi\nu_0 t) \\ &\sim \sin\left(\frac{\pi}{2}\frac{A}{V_\pi}\cos(\phi(t))\right)\cos(2\pi\nu_0 t) \end{aligned} \quad (8)$$

where ν_0 denotes the optical frequency. Based on the same constraints as before, we expand this equation into a Fourier series with the second harmonic term

$$E_{\rm opt}(t) \sim 2J_1\left(\frac{\pi A}{2V_\pi}\right)\cos\left(\phi(t)\right)\cos(2\pi\nu_0 t). \quad (9)$$

From the last expression, we obtain the simple proportionality

$$E_{\rm opt}(t) \sim \cos\left(2\pi\nu_0 t + \phi(t)\right) + \cos\left(2\pi\nu_0 t - \phi(t)\right). \quad (10)$$

Equation (10) represents a double-sideband amplitude modulation with suppressed carrier (AM-DSSC) of the laser light as it can be observed on an optical spectrum analyzer. Both optical frequency components at $\nu_0 \pm f_c/2$ are derived from the same LD and, therefore, the phase noise on each of them is totally correlated and leads to an almost perfect compensation of the millimeter-wave carrier phase fluctuations. Subsequently, the resulting bandwidth of signal $u_{\rm c}(t)$ after detection is governed by the bandwidth of the electrical signal $u_{\rm sc}(t)$ only [11].

The laser light supplied to the Rx module is modulated by the pure LO signal at $f_c/2$ (Fig. 1) in the second MZI. Obviously, the equations given above hold with $u(t) = 1$. The PD in the Rx module detects a coherent reference signal, which can be used for down-conversion of each received signal $y_{m{\rm c}}(t)$ from the mth antenna element. The complex baseband signals $y_m(t)$ are transferred to the control unit by means of two standard coaxial cables, one for the real part and one for the imaginary part and then sampled with four samples per PN code chip. The digitizer stores the uncompressed raw data in a fast acquisition memory of high capacity, which allows an offline postprocessing of the measured data.

In the following, we introduce the complex CIR $h(t, \tau)$ of a time-variant radio channel that depends on the time t and delay τ. ECHO 24 is designed to obtain at a certain time t, an estimation $h_1(\tau)$ of the complex CIR from each antenna element by a simple periodic cross-correlation of $y_m(t)$ with the PN code $u(t)$. This operation can be done efficiently in the frequency domain making use of the Fourier transform $F\{.\}$

$$h_1(\tau) = F^{-1}\{Y_m(f) \cdot U(-f)\} \quad (11)$$

with $Y_m(f) = F\{y_m(t)\}$ and $U(f) = F\{u(t)\}$.

Postprocessing allows also the implementation of inverse filters, which, contrary to the channel estimator in (11), can cope with some nonideal properties of the channel sounder. Details will be discussed in Section IV. An estimation of the complex CIR with inverse filters can be implemented as follows [13]:

$$h_2(\tau) = F^{-1}\{Y_m(f) \cdot H_{\rm inv}(f)\} \quad (12)$$

with

$$H_{\mathrm{inv}}(f) = \begin{cases} 0, & \text{if } Y_{\mathrm{cal}}(f) = 0 \\ \dfrac{1}{Y_{\mathrm{cal}}(f)}, & \text{otherwise} \end{cases}$$

and $Y_{\mathrm{cal}}(f) = F\{y_{\mathrm{cal}}(t)\}$. The calibration function $y_{\mathrm{cal}}(t)$ results from a measurement with a short circuit between the Tx and Rx modules. We refer to such a measurement as a calibration measurement.

In order to get insight into the time- and frequency-dispersion characteristics of the channel, the so-called scattering function [3] is introduced, where ν denotes the Doppler frequency

$$S(\nu, \tau) := E\left[|s(\nu, \tau)|^2\right]. \tag{13}$$

The delay Doppler-spread function $s(\nu, \tau)$ results from the Fourier transform

$$s(\nu, \tau) = F_{t \to \nu}\{h(t, \tau)\}. \tag{14}$$

Equation (13) holds for wide-sense stationary channels with uncorrelated scatterers (WSSUS) only. A good estimate of $S(\nu, \tau)$ can be found employing Welch's method [14].

For postprocessing of the array measurement the space alternating generalized expectation (SAGE) maximization algorithm [15] offers a high-resolution estimation scheme for the complex amplitude, delay, azimuth, and elevation of the impinging partial waves [16]. The SAGE algorithm is based on maximum likelihood estimation and solves the multidimensional maximization problems by a suboptimal iteration procedure.

III. IMPLEMENTATION

A. Control Unit

Due to the fiber-optic connection to the Tx and Rx, the control unit, which consists of rather heavy equipment (computer, monitor, power supply, etc.) placed on a small vehicle can be located far apart from the measurement area. Hence, the investigated electromagnetic fields are not deformed due to a change of the environmental geometry.

In order to transmit a wide-band signal with 1-GHz bandwidth a very fast PN code generator is needed (Fig. 1). The PN code sequence $u(t)$ has a length $N_{\mathrm{c}} = 1023$ and a chip duration $T_{\mathrm{c}} = 2$ ns. Thus, the period time equals $T_a = N_{\mathrm{c}} T_{\mathrm{c}} = 2.046\ \mu$s. The PN code generator is phase-locked to an 10-MHz reference source (RS).

As pointed out before, the digitizer stores uncompressed raw data in its fast acquisition memory. Real and imaginary parts are oversampled twice with a resolution of 8 b/sample. This gives rise to an enormous data stream of 2×2 GB/s. With 8 MB of fast acquisition memory, only short-term measurements can be performed. The digitizer at hand is able to store 2×400 snapshots of length 10 kB. Highly time-variant scenarios with Doppler frequencies of $<$200 Hz that correspond to objects moving at a speed of about 2.5 m/s are continuously observable during a time interval up to only 1 s. Long-term measurements are possible on condition that the time between the snapshots is long enough to transfer the acquired data to the hard disk of the digitizer. The digitizer is also phase-locked to the RS (Fig. 1). Thus, an efficient synchronization of the samples can be achieved. The whole measurement procedure, as well as the bias voltage adjustment for the MZIs, are computer controlled.

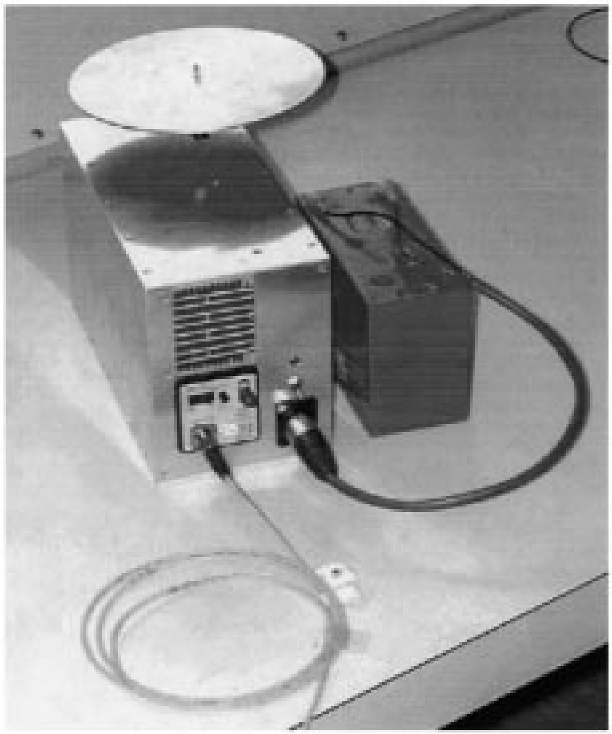

Fig. 2. Tx module with a simple wide-band monopole antenna.

B. Tx Module

The Tx module consists neither of a mixer, nor of a frequency multiplier. Since the desired RF signal is available directly after the PD, only a bandpass amplifier is needed. The opto-electrical conversion causes a considerable powerloss. With an optical input power of 0.5 mW, the electrical power after the detection has −31 dBm only. With 3 dB more optical power, an increase of 6 dB of the electrical power results according to (6). Therefore, the optical output power of the LD (Fig. 1) should be as high as possible with respect to the limits of the MZI and the PD. Polarization maintaining fibers have been chosen for optimum connections between the LD and MZI. The huge amplification of the electrical signal gives no rise to any problems due to the excellent SNR after the PD. The SNR of the LO signal equals 87 dB. For the unmodulated signal after the PD, the SNR equals 80 dB, i.e., only 7 dB are lost.

If the active components of the Tx module are powered by a 12-V battery, a simple fiber connection to the control unit is necessary. Fig. 2 shows the compact Tx module with the battery, the fiber-optic cable, and a single wide-band monopole antenna.

C. Rx Module

The structure of the Rx module is given in Fig. 3. The received signal $y_{mc}(t)$ is either rather weak because of the considerable attenuation in the radio channel at 24 GHz or quite strong if the Tx and Rx antennas are placed near to each other. Hence, the attenuator allows to manually adjust the input power. In order to keep the Rx module small, it would be preferable to displace the

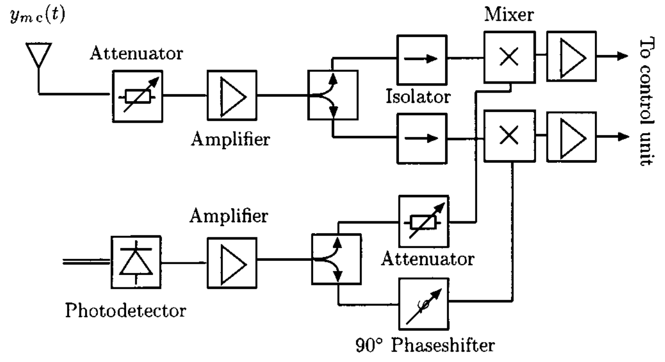

Fig. 3. Block diagram of the Rx module.

down-conversion of the received signal to the control unit. As mentioned before, this is not possible because of the high attenuation of coaxial cables at 24 GHz. Therefore, $y_{mc}(t)$ has to be mixed down to the baseband in the Rx module: once for the real part and once for the imaginary part of the complex CIR. The coherent reference carrier is provided optically by the control unit. The two baseband signals with a bandwidth up to 500 MHz are fed to the control unit by two standard coaxial cables. In spite of the necessity to accommodate the down-conversion in the Rx front-end, the dimensions of the Rx module are increased only by a factor of about two compared to those of the Tx module.

D. Antenna

The element of the antenna array is a wide-band $\lambda/4$ monopole. The corresponding radiation pattern (azimuth ϕ, elevation ϑ) has been approximated in the least-square sense by the fourth-order polynomial

$$f(\phi, \vartheta) = f(\vartheta) = 0.67 + 2.67\vartheta - 6.79\vartheta^2 + 5.74\vartheta^3 - 1.71\vartheta^4$$

which is in good agreement with reality. The variation of the gain stays within ±1 dB from 23.5 to 24.5 GHz.

At present, the antenna array is realized on a virtual basis, i.e., the wide-band $\lambda/4$ monopole moves step by step on a motor driven platform along the coordinates of m array element positions. At each step, a CIR measurement is performed. Of course, such a device operates rather slowly and, therefore, this procedure applies to almost time-invariant channels only. On the other hand, the signal processing is simplified due to the lack of coupling effects between the array elements.

IV. SYSTEM PERFORMANCE

A. CIR Estimation

To demonstrate the performance of the implemented channel estimators correlator (11) and inverse filter (12), the CIR of an ideal channel $h_0(\tau) = \delta(\tau)$ is estimated. Such a CIR results from a measurement with a short circuit between the Tx and Rx modules, which resembles a calibration measurement. The received signal in the frequency domain $Y_m(f)$ equals $\tilde{Y}_{\text{cal}}(f)$, a realization of $Y_{\text{cal}}(f)$ with different noise.

According to (11), $h_{10}(\tau)$ is obtained replacing $Y_m(f)$ by $\tilde{Y}_{\text{cal}}(f)$. Considering $h_{10}(\tau)$ in Fig. 4, the main correlation peak has an expected halfwidth of 2 ns but is not perfectly triangular.

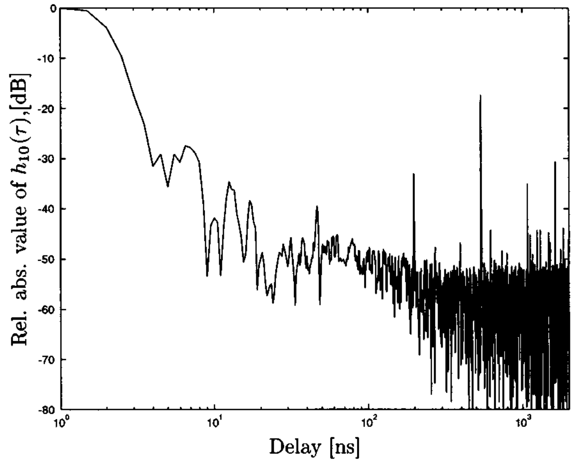

Fig. 4. Estimate of $h_0(\tau) = \delta(\tau)$ obtained with a correlator.

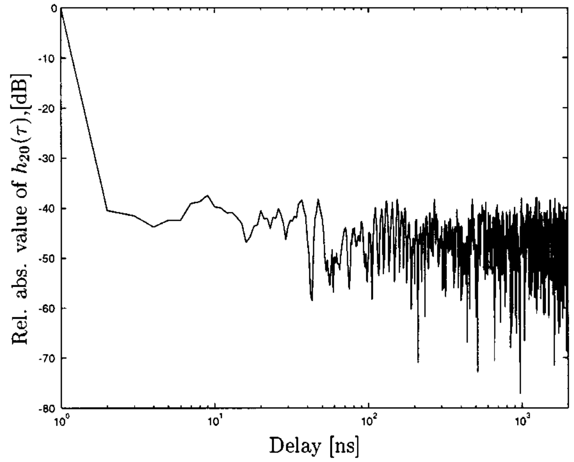

Fig. 5. Estimate of $h_0(\tau) = \delta(\tau)$ obtained with an inverse filter.

Moreover, several additional correlation peaks appear, an especially strong one at about 550 ns. Still, if the delay spread in an indoor situation stays below 550 ns, this estimation method yields a good approximation.

With the inverse filter according to (12), $h_{20}(\tau)$, a second estimation of $h_0(\tau) = \delta(\tau)$, results. Again, $Y_m(f)$ is replaced by a $\tilde{Y}_{\text{cal}}(f)$. In order keep the noise of the inverse filter process low, the calibration function $y_{\text{cal}}(t)$ is low-pass filtered with a bandwidth of $\leq$500 MHz and values smaller than a certain threshold value are set to one. The distortions induced by the system are compensated, as illustrated in Fig. 5. The main correlation peak becomes almost ideal with a halfwidth of 1 ns.

The estimation with the correlation filter exhibits an SNR of 55 dB, which we refer to as dynamic range of the channel sounder. An improvement of the dynamic range could be achieved by averaging several periods of the calibration function $y_{\text{cal}}(t)$. With the inverse filter method, an SNR of 45 dB results, i.e., a 10-dB loss of SNR must be taken into account.

When estimating amplitude and phase with the implemented high-resolution algorithm based on SAGE, the nonideal properties of the system are compensated as well if the algorithm is provided with the calibration function $y_{\text{cal}}(t)$.

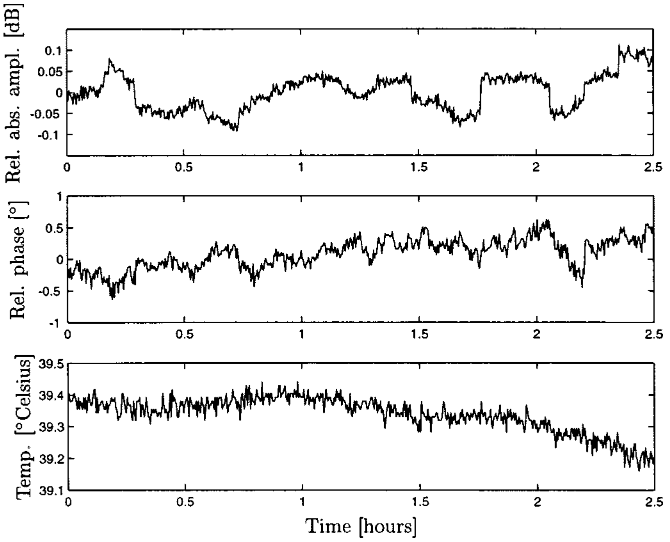

Fig. 6. Long-term variation with constant temperature.

B. Stability

To investigate the overall stability of ECHO 24, the variation of the correlation peak of many CIRs of an $\delta(\tau)$ channel has been observed. Although the demodulation of the received signal should be performed coherently and the 12-GHz oscillator is phase locked to the 10-MHz RS, the systems impulse response depends on the temperature variations of the system components, especially of the two MZIs. During the 1-h warm-up time of the system, amplitude and phase of the correlation peak change significantly. Afterwards, the temperature of the environment may still change. Thus, e.g., with a nearly linear increase and decrease of about 1 °C over more than 1 h, the absolute amplitude fluctuates within ± 0.2 dB and the phase steps within $\pm 2°$. If the temperature is more or less constant, the variation of the absolute amplitude and the phase stay within ± 0.15 dB and $\pm 1°$, respectively (Fig. 6). Hence, for long-term measurements the temperature has to be kept constant or the system needs to be recalibrated from time to time. For short-term measurements, e.g., for array measurements, the temperature is supposed to be stable and subsequently, the variation stays within ± 0.05 dB for the amplitude and $\pm 0.5°$ for the phase. The high-resolution estimation of amplitude and angle of incidence are not affected by such small fluctuation, as demonstrated in Section V.

V. MEASUREMENTS

In this section, three different measurements performed with ECHO 24 are presented. First, a displacement-triggered measurement of a time-invariant channel is given. A second example demonstrates the influence of fluorescent lights on the CIR. The results show the ability of the ECHO 24 equipped with a single $\lambda/4$ monopole antenna to cope with highly time-variant radio channels and Doppler frequencies. Finally, an array measurement in a predetermined time-invariant scenario delivers the necessary data to prove the high-resolution estimation of the parameters characterizing the impinging waves, i.e., the complex amplitude, delay, incidence azimuth, and incidence elevation.

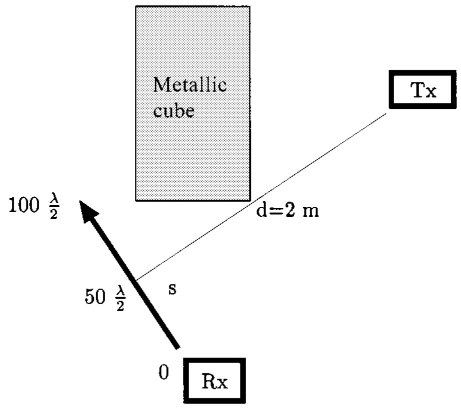

Fig. 7. Measurement site according to scenario 1 (top view).

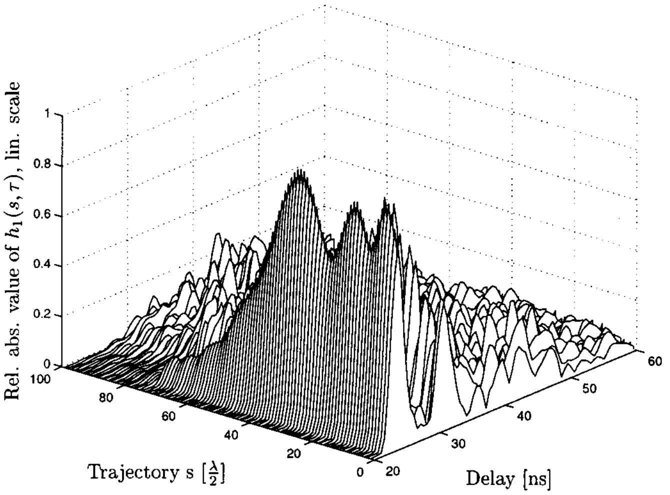

Fig. 8. Displacement-triggered measurement of the CIR (scenario 1).

The first scenario is depicted in Fig. 7. The Rx antenna is moved along the trajectory s, while the Tx antenna remains at its position. At every trajectory point $\lambda/2$, a measurement is triggered. At the halfway point, i.e., after $50 \cdot \lambda/2$, the Rx antenna looses line of sight (LOS) and moves into the shadow zone of the metallic cube. According to Fig. 8, the absolute maximum values of the LOS path occur at a delay of 24 ns. At the halfway point, the LOS shows only half the amplitude and then vanishes monotonously to zero. The oscillation of the amplitude before the halfway point can be explained by the partially shadowing in the Fresnel zones, as known from wave propagation theory. Such measurements might be useful to investigate diffraction effects.

The second measurement deals with the fading effect due to a fluorescent light tube. The plasma inside fluorescent light tubes reflects the waves at twice the frequency of the power net, i.e., at 100 Hz, as reported earlier in [17]. Fig. 9 represents a sketch of the measurement setup. A metallic sheet attenuates the direct path in order to emphasize the reflected path with fast fading. The measurement consists of 100 snapshots, which are triggered in intervals of 1.37 ms. The absolute value of the resulting complex CIR is shown in Fig. 10. At a delay of 31 ns, a maximum of periodic fluctuation can be observed. At a first glance, we

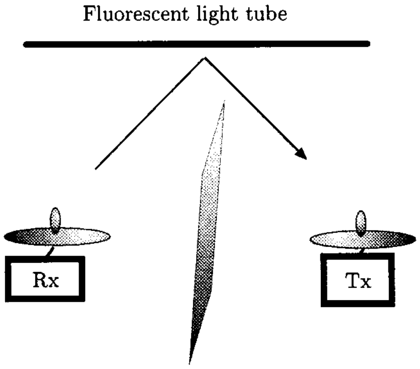

Fig. 9. Measurement site according to scenario 2.

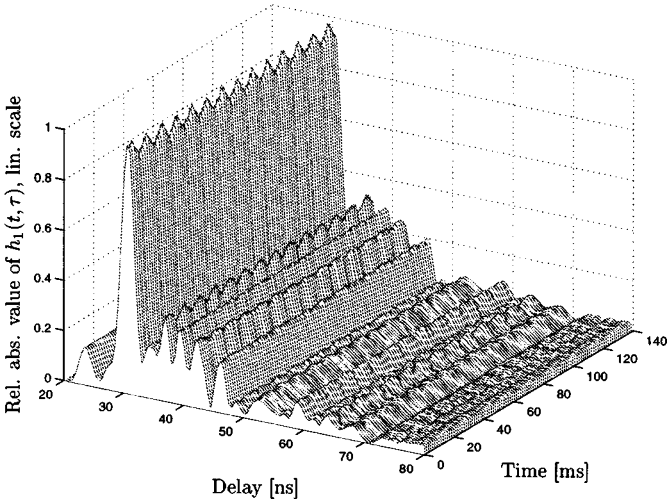

Fig. 10. CIR influenced by a fluorescent light (scenario 2).

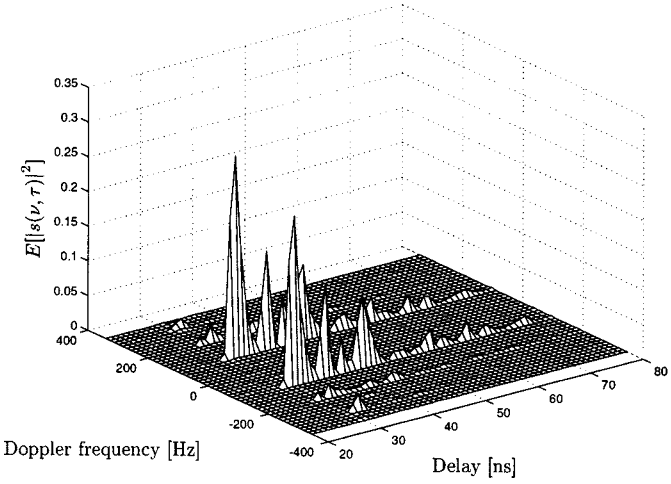

Fig. 11. Estimated scattering function (scenario 2).

count about 13.5 periods during 137 ms. A more detailed analysis yields the scattering function calculated according to (13). The result is depicted in Fig. 11. Expectedly, at a delay of 31 ns, the spectrum exhibits a maximum peak at ±100 Hz.

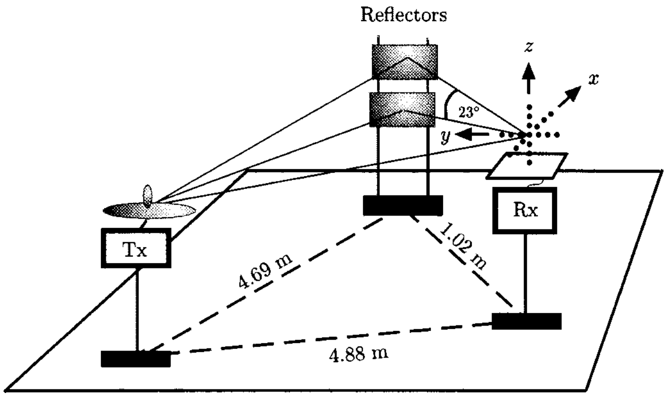

Fig. 12. Array measurement site according to scenario 3.

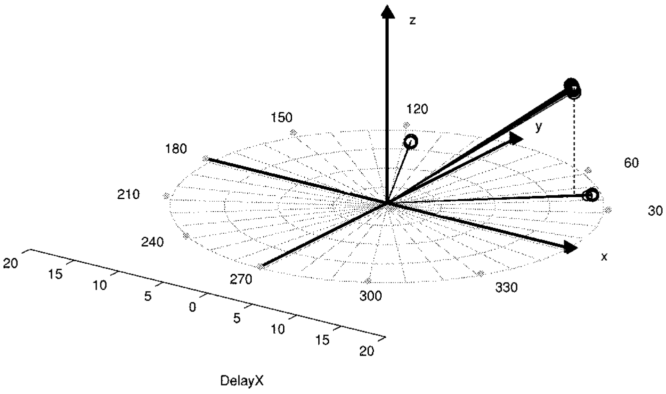

Fig. 13. Array measurement of delays, azimuth, and elevation angles (scenario 3).

TABLE I

ANALYSIS OF THE MEASUREMENT RESULTS OBTAINED IN THE SCENARIO 3

Propagation path	direct path	upper reflector	lower reflector
Delays:			
Reference [ns]	16.2173	19.1532	19.0406
Average [ns]	16.0167	19.0	19.0
Standard deviation [ns]	0.0913	0.0	0.0
Azimuth angles:			
Reference [°]	117.7043	46.454	43.3319
Average [°]	117.3920	46.17	41.1903
Standard deviation [°]	0.0491	0.1353	0.2341
Elevation angles:			
Reference [°]	−0.448	23.4655	0.1783
Average [°]	0.0	23.827	0.0
Standard deviation [°]	0.0	0.3325	0.0

Finally, the measurement in a predetermined incidence constellation according to Fig. 12 with an LOS path and two reflected paths demonstrates the reliability of ECHO 24 and the high-resolution estimation scheme based on the SAGE algorithm. The array measurements are performed outdoors where no other reflecting or scattering objects are present. The radio channel is assumed to be time invariant during the measurements. The exact positions of Rx, Tx, and the two reflectors are determined by measurements with a theodolite. The reflectors, two 56 × 25 cm copper sheets, are installed on top of each other. Thus, the incidence delays and azimuths of the reflected waves are nearly equal while the elevations have different values.

For this measurement, a three-dimensional (3-D) uniform cross array consisting of 11 wide-band $\lambda/4$ monopoles equispaced in each direction with an interelement distance of $\lambda/2$ has been used. The successive measurements in the 33 positions takes about 3 min. The measurements have been repeated 30 times within 1.5 h. Fig. 13 illustrates the estimated delays, azimuths, and elevations and their variations. An inspection of Table I shows that all mean values of the delay, azimuth, and elevation estimates are close to the reference values obtained by means of theodolite measurements. In all but one measurement, the delay estimates lie correctly within the 0.5-ns quantization grid. The azimuth and elevation estimates of the direct wave have an average limited by the precision of the theodolite ($\pm 0.5^\circ$). For the reflected waves, an additional deviation occurs because the reflecting points could not be determined exactly and, thus, were assumed to be located in the middle of the reflector sheets. Note that the resolution with respect to the elevation angle enables the separation of two waves having nearly equal delays and azimuth. The empirical standard deviation of all azimuth and elevation estimates is less than 0.4°. For an incidence elevation close to zero, an elevation of 0° is estimated in all measurements because the small phase differences of the antenna signals cannot be resolved by the digitizer.

VI. CONCLUSIONS

The accurate measurement of complex radio CIRs requires the exact knowledge of the carrier phase at the Rx input of the sounder system. In case of time-variant channels, an online synchronization between the Tx and Rx is inevitable. At millimeter-wave frequencies, neither a coaxial connection nor a atomic standard control of the Tx and Rx oscillator can be used due to the prohibitive line attenuation, as well as the impossibility to achieve a sufficient degree of coherence. The novel synchronization scheme of ECHO 24 based on the fiber-optic transmission of an appropriately modulated lightwave reveals to be a handy and robust solution of the problem. Moreover, the involved optic millimeter-wave generation principle permits the realization of rather small Tx and Rx modules, which, in turn, deform the electromagnetic-field pattern very slightly and, therefore, increase the accuracy of the measurements.

Fiber-optic signal transmission offers also a very large bandwidth in the millimeter-wave ranges. Thus, ECHO 24 has a 2-ns delay resolution, which is well suited for indoor measurements. Equipped with a single $\lambda/4$ monopole antenna, subsequent CIR measurements can be performed every 2 μs. Hence, it is possible to analyze strongly time-variant channels. Using an antenna array information on the incident angels of the impinging partial waves can also be obtained. For this purpose, powerful signal-processing methods are required. Actually, the array measurement is simulated by successive measurements with a single antenna element at the corresponding positions and lasts 3 min for 33 steps. It goes without saying that such a procedure can be applied for the investigation of time-invariant channels only. A 2-D uniform cross patch antenna array with 16 elements will be operational soon. This device permits the measurement of several path CIRs and the corresponding angles of arrival within 64 μs.

The described measurements in the three different scenarios give some insight into the versatility and capability of ECHO 24 with regard to the complex amplitude, delay, angle, and time resolution. Several measurement campaigns are performed in order to collect a huge amount of data, which allow the determination of accurate parameter sets for reliable stochastic radio channel models.

ACKNOWLEDGMENT

The authors would like to express their thanks to M. Tschudin, Communication Technology Laboratory, Swiss Federal Institute of Technology, Zurich, Switzerland, H. Jäger, Communication Technology Laboratory, Swiss Federal Institute of Technology, Zurich, Switzerland, C. Schmid, Communication Technology Laboratory, Swiss Federal Institute of Technology, Zurich, Switzerland, and R. Heddergott, Communication Technology Laboratory, Swiss Federal Institute of Technology, Zurich, Switzerland, for their theoretical and practical contributions over the last years to the development of the channel sounder and, in particular, for their assistance during the preparation of this paper.

REFERENCES

[1] R. Prasad, "Overview of wireless personal communications: Microwave perspectives," *IEEE Commun. Mag.*, vol. 35, pp. 104–108, Apr. 1997.
[2] R. Prasad, J. S. Dasilva, and B. Arroyo-Fernández, "ACTS mobile programme in Europe," *IEEE Commun. Mag.*, vol. 36, pp. 80–81, Feb. 1998.
[3] P. A. Bello, "Characterization of randomly time-variant linear channels," *IEEE Trans. Commun. Syst.*, vol. CS-11, pp. 360–393, Dec. 1963.
[4] H. Krim and M. Viberg, "Two decades of array signal processing research," *IEEE Signal Processing Mag.*, pp. 67–94, July 1996.
[5] B. H. Fleury, D. Dahlhaus, R. Heddergott, and M. Tschudin, "Wide-band angle of arrival estimation using the SAGE algorithm," in *Proc. IEEE 4th Int. Symp. Spread-Spectrum Tech. Applicat.*, Mainz, Germany, Sept. 1996, pp. 79–85.
[6] P. F. M. Smulders and A. G. Wagemans, "Wideband indoor radio propagation measurements at 58 GHz," *Electron. Lett.*, pp. 1270–1271, June 1992.
[7] R. Davies, M. Bensebti, M. A. Beach, and J. McGeehan, "Wireless propagation measurements in indoor multipath environments at 1.7 GHz and 60 GHz for small cell systems," in *Proc. IEEE Veh. Technol. Conf.*, May 1991, pp. 589–593.
[8] B. H. Fleury and P. E. Leuthold, "Radiowave propagation in mobile communications: An overview of European research," *IEEE Commun. Mag.*, vol. 34, pp. 70–81, Feb. 1996.
[9] G. Løvnes, S. E. Paulsen, and R. H. Rækken, "A versatile channel sounder for millimeter wave measurements," in *Proc. 4th IEEE Int. Symp. Personal, Indoor, Mobile Radio Commun.*, Yokohama, Japan, Sept. 1993, pp. 382–386.
[10] U. Dersch and E. Zollinger, "Physical characteristics of urban micro-cellular propagation," *IEEE Trans. Antennas Propagat.*, vol. 42, pp. 1528–1539, Nov. 1994.
[11] J. O'Reilly, P. Lane, R. Heidemann, and R. Hofstetter, "Optical generation of very narrow linewidth millimeter wave signals," *Electron. Lett.*, vol. 30, pp. 59–60, Jan. 1990.
[12] C. Tocci and J. Caulfield, *Optical Interconnection: Foundations and Applications*. Norwood, MA: Artech House, 1994.
[13] U. Martin, "Ausbreitung in Mobilfunkkanalen: Beitrage zum Entwurf von Messgeraten und zur Echoschaatzung," Ph.D. dissertation, Telecommun. Lab, Univ. Erlangen-Nuremberg, Erlangen, Germany, 1994.
[14] S. M. Kay, *Modern Spectral Estimation, Theory and Applications*. Englewood Cliffs, NJ: Prentice-Hall, 1988.
[15] J. A. Fessler and A. O. Hero, "Space-alternating generalized expectation-maximization algorithm," *IEEE Trans. Signal Processing*, vol. 42, pp. 2664–2677, Oct. 1994.
[16] M. Tschudin, R. Heddergott, and P. Truffer, "Validation of a high resolution measurement technique for estimating the parameters of impinging waves in indoor environments," in *Proc. IEEE Int. Personal, Indoor, Mobile Radio Commun.*, Sept. 1998, pp. 1411–1426.
[17] P. Melançon and J. Lebel, "Effects of fluorescent lights on signal fading characteristics for indoor radio channels," *Electron. Lett.*, vol. 28, pp. 1740–1741, Aug. 1992.

Pascal Truffer (S'96) was born in Zurich, Switzerland, on May 10, 1968. He received the Diploma degree in electrical engineering from the Swiss Federal Institute of Technology (ETH) Zurich, Zurich, Switzerland, in 1994.

He then joined the Communication Technology Laboratory, ETH Zurich, where he is currently engaged in research on experimental assessment of millimeter-wave propagation properties in indoor environments.

Peter E. Leuthold (M'68) received the Diploma and Ph.D. degrees in electrical engineering from the Swiss Federal Institute of Technology (ETH) Zurich, Zurich, Switzerland, in 1962 and 1967, respectively, and the Habilitation degree from the ETH in 1971.

From 1964 to 1967, he was an Associate Member of the Technical Staff at Philips Research Laboratories, Eindhoven, Netherlands. In 1968, he joined the Research Staff of the High Frequency Electronics Laboratory, ETH Zurich, where he worked on multidimensional digital filter structures and their application in data modems. From 1974 to 1977, he was a Full-Time Lecturer at the Intercantonal Engineering College, Rapperswil, Switzerland. Since Fall 1977, he has been a Professor at ETH Zurich, where he is also Head of the Communication Technology Laboratory. His research interests include mobile radio communications and fiber-optical networks.

Dr. Leuthold has organized several international conferences on telecommunications and electromagnetic compatibility and was general chairman of ICC'93, Geneva, Switzerland.